Organometallic Mixed-Valence Systems. Two-Center and Three-Center Compounds with *meta* Connections around a Central Phenylene Ring

Tania Weyland,[†] Karine Costuas,[‡] Loic Toupet,[§] Jean-François Halet,*[,‡] and Claude Lapinte*[,†]

Organométalliques et Catalyse, UMR CNRS 6509, and Laboratoire de Chimie du Solide et Inorganique Moléculaire, UMR CNRS 6511 of the Institut de Chimie de Rennes, and Groupe Matière Condensée et Matériaux, UMR CNRS 6626, Université de Rennes 1, Campus de Beaulieu, 35042 Rennes Cedex, France

Received April 21, 2000

The bi- and trinuclear mixed-valence complexes [{Cp*(dppe)Fe(CC−)}$_2$(1,3-C$_6$H$_4$)][PF$_6$] (**2**$^+$), [{Cp*(dppe)Fe(CC−)}$_3$(1,3,5-C$_6$H$_3$)][PF$_6$] (**3**$^+$), and [{Cp*(dppe)Fe(CC−)}$_3$(1,3,5-C$_6$H$_3$)][PF$_6$]$_2$ (**3**$^{2+}$) were prepared either by oxidation of [{Cp*(dppe)Fe(CC−)}$_2$(1,3-C$_6$H$_4$)] (**2**) or [{Cp*-(dppe)Fe(CC−)}$_3$(1,3,5-C$_6$H$_3$)] (**3**) with 1 or 2 equiv of [(C$_5$H$_5$)$_2$Fe][PF$_6$] or by reaction between the homovalent species **2** and **2**$^{2+}$ or **3** and **3**$^{3+}$. After crystallization (CH$_2$Cl$_2$/pentane) at −20 °C, the mixed-valence complexes **2**$^+$, **3**$^+$, and **3**$^{2+}$ were isolated in good yields (80−93%). The well-resolved separations between the redox processes in the cyclic voltammograms enabled computation of the comproportionation constants (K_c) and the molar fraction (x^{n+}) for all the species **2**$^{n+}$ (n = 0, 1, 2) and **3**$^{n+}$ (n = 0, 1, 2, 3) present in solution. The X-ray crystal structure of **2**$^+$ revealed that the two iron atoms are not equivalent, suggesting localized Fe(II) and Fe(III) sites. IR, Mössbauer, ESR, and UV−vis spectroscopies also provide evidence for localized oxidation states. Analyses of the NIR spectra showed both a forbidden ligand field transition specific to the Cp*(dppe)Fe(III) fragment and a unique ICT band for the weakly coupled mixed-valence system **2**$^+$ and **3**$^+$ (V_{ab} = 161 and 143 cm^{-1}, respectively). In the case of the diradical trinuclear mixed-valence **3**$^{2+}$, two distinct ICT bands were observed and attributed to the two possible independent ways to transfer an electron in the singlet and triplet states of such a mixed-valence compound. Density functional molecular orbital calculations provide the electronic structure of these mixed-valence systems.

Introduction

In previous papers we described the synthesis and the physical properties of organometallic molecules of general formula [{Cp*(dppe)Fe−C≡C−)$_x$C$_6$H$_{6-x}$]^{n+}n[PF$_6$] ($1 < x < 3$) containing one (**1**$^{n+}$, n = 0, 1), two (**2**$^{n+}$, n = 0, 2), and three (**3**$^{n+}$, n = 0, 3) Cp*Fe(dppe) building blocks connected through an ethyndiyl spacer with a rigid *m*-phenylene framework.[1,2] As the organoiron fragments are stable as both 18-electron iron(II) and 17-electron iron(III), it was possible to isolate these complexes as diamagnetic neutral species and as polyradicals. In particular, we have reported that the bi- and triradicals present a ferromagnetic coupling with a magnetic interaction of significant strength at nanoscale distances. In the binuclear complex the ferromagnetic interaction produces a triplet ground state ($2J$ = 130.6 cm^{-1}). In the triradical species, two doublet states lie above the quartet ground state by 18.7 and 28.8 cm^{-1}.

This paper is devoted to the synthesis and study of the organometallic mixed-valence (MV) systems (**2**$^+$, **3**$^+$, and **3**$^{2+}$) with the same topology as **2**$^{2+}$ and **3**$^{3+}$. These models allow interesting comparisons between the two-redox-site one-electron MV Fe(II)−Fe(III) (**2**$^+$), the three-redox-site one-electron Fe(II)−Fe(II)−Fe(III) (**3**$^+$), and three-redox-site two-electron MV systems Fe(II)−Fe(III)−Fe(III) (**3**$^{2+}$). Considering an equilateral triangular system with three site orbitals a, b, c and five electrons (Scheme 1), one electron on one of the doubly occupied sites b and c can move to the singly occupied site a. This is a classical case of electron transfer, and a unique electronic coupling parameter is expected (V_{ab} = V_{ac}). Suppose now that there are only four electrons on the three sites, two of them unpaired and occupying neighboring sites, which can interact. Depending on the ferromagnetic ($J > 0$) or antiferromagnetic ($J < 0$) nature of their coupling, two different situations are possible. It appears that the magnetic interaction between the sites a and b may induce a perturbation of the electronic coupling for the electron transfer from c toward a and b. In this case, the pair of electronic coupling parameters (V_{bc1} = V_{ac1}) and (V_{bc2} = V_{ac2}) is

* Corresponding author. E-mail: lapinte@univ-rennes1.fr.
[†] Organométalliques et Catalyse, UMR CNRS 6509, Institut de Chimie de Rennes.
[‡] Laboratoire de Chimie du Solide et Inorganique Moléculaire, UMR CNRS 6511, Institut de Chimie de Rennes.
[§] Groupe Matière Condensée et Matériaux, UMR 6626.

(1) Weyland, T.; Lapinte, C.; Frapper, G.; Calhorda, M. J.; Halet, J.-F.; Toupet, L. *Organometallics* **1997**, *16*, 2024.
(2) Weyland, T.; Costuas, K.; Mari, A.; Halet, J.-F.; Lapinte, C. *Organometallics* **1998**, *17*, 5569.

10.1021/om000341l CCC: $19.00
Publication on Web 09/08/2000

Scheme 1

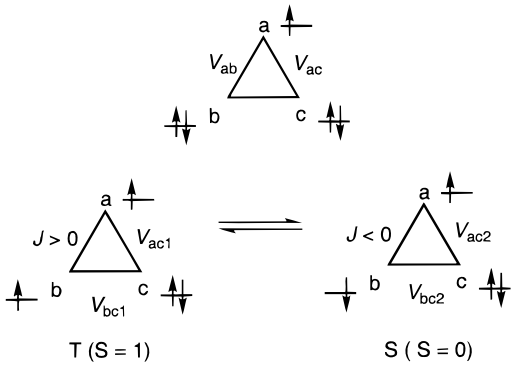

not expected to be equivalent. The mixed-valence complexes $\mathbf{3}^+$ and $\mathbf{3}^{2+}$ constitute a simple case to study experimentally and theoretically the interplay between electron exchange and electron transfer.

These fundamental processes are relevant both to devices for molecular electronics[3,4] and to electron-transfer processes in proteins with multi-redox sites.[5] Besides numerous examples of mixed-valence compounds with infinite structure in inorganic solid-state chemistry, most of the work devoted to mixed-valence systems deals with symmetrical, delocalized organic molecules containing two identical redox-active termini.[4,6−8] The synthetic mixed-valence systems with more than two redox-active centers are rare.[9−11] Several trinuclear complexes linked with a *meta*-phenylene unit have been synthesized. However, no in-depth investigation has been conducted on the interaction between the metal centers in these molecules.[12−19]

We report here (i) the study of the comproportionation equilibrium between the components of the system on the basis of electrochemical data previously obtained with the neutral precursors, (ii) the synthesis and isolation of the bi- and trinuclear mixed-valence complexes $[\{Cp^*(dppe)Fe(C{\equiv}C-)\}_2(1,3\text{-}C_6H_4)][PF_6]$ ($\mathbf{2}^+$), $[\{Cp^*(dppe)Fe(C{\equiv}C-)\}_3(1,3,5\text{-}C_6H_3)][PF_6]$ ($\mathbf{3}^+$), and $[\{Cp^*(dppe)Fe(C{\equiv}C-)\}_3(1,3,5\text{-}C_6H_3)][PF_6]_2$ ($\mathbf{3}^{2+}$), (iii) the X-ray crystal structure of $\mathbf{2}^+$, (iv) the full spectroscopic characterization of the mixed-valence complex, which establishes that the electron motion from one metal site to another is slow, (v) the study of the intervalence charge transfer band (ICT) in the NIR range, which clearly reveals that two different electron-transfer processes operate in $\mathbf{3}^{2+}$, and (vi) the electronic structures of these open-shell derivatives obtained from density functional (DF) calculations.

Table 1. Comproportionation Constants and Molar Fraction of the Species (x^{n+}) Present in Solution at 20 °C

compd	$\Delta E°_1$[a]	$\Delta E°_2$[a]	K_{c1}[b]	K_{c2}[b]	x	x^+	x^{2+}	x^{3+}
$\mathbf{2}^+$	0.125		130		0.154	0.691	0.154	
$\mathbf{3}^+$	0.125	0.125	130	130	0.075	0.850	0.075	<0.001
$\mathbf{3}^{2+}$	0.125	0.125	130	130	<0.001	0.075	0.850	0.075
$\mathbf{4}^+$	0.260		2.55×10^4		0.043	0.935	0.043	

[a] $\Delta E° = E°_1 - E°_2$ (in V) obtained from cyclic voltammetry on a Pt electrode at 20 °C in CH_2Cl_2 containing 0.1 M NBu_4PF_6. [b] From $\Delta E_0 = (RT/F) \ln K_c$ at 20 °C.

Results and Discussion

1. Determination of the Comproportionation Constants. The cyclic voltammograms for the binuclear complex **2** and the trinuclear derivative **3** are characterized by two or three reversible waves, respectively.[1] The separations ($\Delta E°$) between the different redox processes were well-resolved and have been determined for both compounds (Table 1).[1] The experimental determination of $\Delta E°$ allows the calculation of the thermodynamic constants ($K_c = \exp(\Delta E°F/RT)$ for the comproportionation equilibria in the case of both the binuclear (eq 1) and trinuclear systems (eqs 2 and 3).

$$\underset{\mathbf{2}}{\text{Fe(II)-L-Fe(II)}} + \underset{\mathbf{2}^{2+}}{\text{[Fe(III)-L-Fe(III)]}^{++}} \overset{Kc1}{\rightleftharpoons} 2\ \underset{\mathbf{2}^{+}}{\text{[Fe(II)-L-Fe(III)]}^{+}} \quad (1)$$

$$\underset{\mathbf{3}}{\text{Fe(II)-L-Fe(II)-L-Fe(II)}} + \underset{\mathbf{3}^{2+}}{\text{[Fe(II)-L-Fe(III)-L-Fe(III)]}^{++}} \overset{Kc1}{\rightleftharpoons} 2\ \underset{\mathbf{3}^{+}}{\text{[Fe(II)-L-Fe(II)-L-Fe(III)]}^{+}} \quad (2)$$

$$\underset{\mathbf{3}^{+}}{\text{[Fe(II)-L-Fe(II)-L-Fe(III)]}^{+}} + \underset{\mathbf{3}^{3+}}{\text{[Fe(III)-L-Fe(III)-L-Fe(III)]}^{+++}} \overset{Kc2}{\rightleftharpoons} 2\ \underset{\mathbf{3}^{2+}}{\text{[Fe(II)-L-Fe(III)-L-Fe(III)]}^{++}} \quad (3)$$

In symmetrical compounds, the potential difference $\Delta E°$ (or the comproportionation constant K_c) is often taken as a measure of the electronic interaction through a given bridge. In fact, this quantity is related to the thermodynamic stability of the MV compound described by the comproportionation equilibrium. It comprises energetic terms other than the through-bridge electronic interaction, such as through-space electrostatic interaction, solvation, steric interaction, or structural distortion upon electron transfer.[4] Considering the *meta*-phenylene topology of the complexes **2** and **3**, the K_c values are rather large.[20−22] Indeed, for many compounds with this topology, much smaller K_c and $\Delta E°$ values have been reported. Note that when $\Delta E°$ is too small to permit the separation of the waves in the cyclic voltammogram, an alternative spectroscopic determination of K_c must be

(3) Lehn, J.-M. *Supramolecular Chemistry−Concepts and Perspectives*; VCH: Weinheim, 1995.
(4) Astruc, D. *Electron Transfer and Radical Processes in Transition-Metal Chemistry*; VCH: New York, 1995.
(5) Blondin, G.; Girerd, J.-J. *Chem. Rev.* **1990**, *90*, 1359.
(6) Robin, M. B.; Day, P. *Adv. Inorg. Chem. Radiochem.* **1967**, *10*, 247.
(7) Hush, N. S. *Trans. Faraday Soc.* **1961**, *57*, 557.
(8) Hush, N. S. *Prog. Inorg. Chem.* **1967**, *8*, 391.
(9) Bonvoisin, J.; Launay, J.-P.; Van der Auweraer, M.; De Schryver, F. C. *J. Phys. Chem.* **1994**, *98*, 5052.
(10) Bonvoisin, J.; Launay, J. P.; Verbouwe, W.; Vanderauweraer, M.; Deschryver, F. C. *J. Phys. Chem.* **1996**, *100*, 17079.
(11) Sedo, J.; Ruiz, D.; Vidalgancedo, J.; Rovira, C.; Bonvoisin, J.; Launay, J. P.; Veciana, J. *Adv. Mater.* **1996**, *8*, 748.
(12) Hunter, A. D.; Szigety, A. B. *Organometallics* **1989**, *8*, 2670.
(13) Buchwald, S. L.; Lucas, E. L.; Davis, W. D. *J. Am. Chem. Soc.* **1989**, *111*, 397.
(14) Hunter, A. D.; MacLenon, J. L. *Organometallics* **1989**, *8*, 2679.
(15) Hunter, A. D. *Organometallics* **1989**, *8*, 1118.
(16) Tykwinski, R.; Stang, P. J. *Organometallics* **1992**, *13*, 3203.
(17) Khan, M. S.; Schwartz, D. J.; Pasha, N. A.; Kakkar, A. K.; Lin, B.; Raithby, P. R.; Lewis, J. *Z. Anorg. Allg. Chem.* **1992**, *616*, 121.
(18) Ohshiro, N.; Takei, F.; Onitsuka, K.; Takahashi, S. *Chem. Lett.* **1996**, 871.
(19) Whittall, I. R.; Humphrey, M. G.; Houbrechts, S.; Maes, J.; Persoons, A.; Schmid, S.; Hockless, D. C. R. *J. Organomet. Chem.* **1997**, *544*, 277.
(20) Fink, H.; Long, N. J.; Martin, A. J.; Opromolla, G.; White, A. J. P.; Williams, D. J.; Zanello, P. *Organometallics* **1997**, *16*, 2646.
(21) Nakashima, T.; Kunitake, T. *Bull. Chem. Soc. Jpn.* **1972**, *45*, 2892.
(22) Beer, P. D.; Crowe, D. B.; Ogden, M. I.; Drew, M. G. B.; Main, B. *J. Chem. Soc., Dalton Trans.* **1993**, 2107.

used, providing less accurate K_c values.[9,10,23] In our case, the strong interaction between the redox units results from linking the metal and the benzene ring with an ethyndiyl spacer, which favors a continuous overlap between the d orbitals of the metal centers and the π orbitals of the polyethynylbenzene connector. The most relevant system discussed in this work is $Cl(depe)_2FeC{\equiv}C\text{-}1,3\text{-}C_6H_4{-}C{\equiv}CFe(depe)_2Cl$ investigated by Long et al.[24,25] These compounds display similar wave separations in the cyclic voltammogram, and therefore the metal−metal interaction should be close in these two families of complexes.

The molar fraction x^{n+} of all the species $\mathbf{2}^{n+}$ ($n = 0$, 1, 2) and $\mathbf{3}^{n+}$ ($n = 0$, 1, 2, 3) present in solution at 25 °C have been computed using the comproportionation constants (Table 1, see Experimental Section). These data confirm that the mixed-valence species predominate in solution. However, the amount of the associated homovalent species is quite appreciable. Interestingly, knowledge of the concentration of the species present in the solution allows accurate determination of the molecular properties such as the molecular extinction coefficient in the UV−vis−NIR spectroscopies. From a synthetic point of view, the position of the comproportionation equilibrium can preclude the isolation of the MV species $\mathbf{2}^+$, $\mathbf{3}^+$, and $\mathbf{3}^{2+}$ as pure compounds. However, as the K_c value increases with the decrease of the temperature, these MV complexes were viewed as accessible synthetic targets at low temperatures.

2. Synthesis of the Mixed-Valence Bi- and Trinuclear Complexes [{Cp*(dppe)Fe(CC−)}$_2$(1,3-C$_6$H$_4$)][PF$_6$] ($\mathbf{2}^+$), [{Cp*(dppe)Fe(CC−)}$_3$(1,3,5-C$_6$H$_3$)][PF$_6$] ($\mathbf{3}^+$), and [{Cp*(dppe)Fe(CC−)}$_3$(1,3,5-C$_6$H$_3$)][PF$_6$]$_2$ ($\mathbf{3}^{2+}$). The neutral iron(II) compounds **2** and **3** were previously obtained by treatment of the iron chloro complex Cp*(dppe)FeCl (**4**) with the bis- or tris-(trimethylsilyl) precursor of the bridging ligands.[1] The di- or tricationic iron(III) compounds $\mathbf{2}^{2+}$ and $\mathbf{3}^{3+}$ were prepared by the oxidation of the corresponding iron(II) homologues with 2 or 3 equiv of ferrocenium.[2] The mixed-valence complexes $\mathbf{2}^+$, $\mathbf{3}^+$, and $\mathbf{3}^{2+}$ can be prepared either from the comproportionation reaction between **2** and $\mathbf{2}^{2+}$ or **3** and $\mathbf{3}^{3+}$ or by the oxidation of **2** and **3** with 1 or 2 equiv of ferrocenium ion (Schemes 2, 3). The electron-transfer reactions were carried out in a CH_2Cl_2 suspension. The deep blue solution formed after a few minutes of reaction was filtered to check that all the material was dissolved, and the solvent was then removed. Complexes $\mathbf{2}^+$, $\mathbf{3}^+$, and $\mathbf{3}^{2+}$ were isolated as thermally stable microcrystals in 95% yield. Purification of the crude material was carried out by crystallization from CH_2Cl_2 by addition of pentane at −20 °C. The mixed-valence complexes $\mathbf{2}^+$, $\mathbf{3}^+$, and $\mathbf{3}^{2+}$ were recovered in good yields ranging from 80 to 93%. In contrast, the precipitation performed at 20 °C gave the blue homoiron(III) species $\mathbf{2}^{2+}$ or $\mathbf{3}^{3+}$ by displacement of the equilibria 1−3 on the left side. The analytically pure salts $\mathbf{2}^+$, $\mathbf{3}^+$, and $\mathbf{3}^{2+}$, which showed the same cyclic voltammograms as their parent compounds **2** and **3** with two and three reversible waves, respectively, were characterized by IR, UV−vis, NIR, Mössbauer, and ESR spectroscopies.

Scheme 2

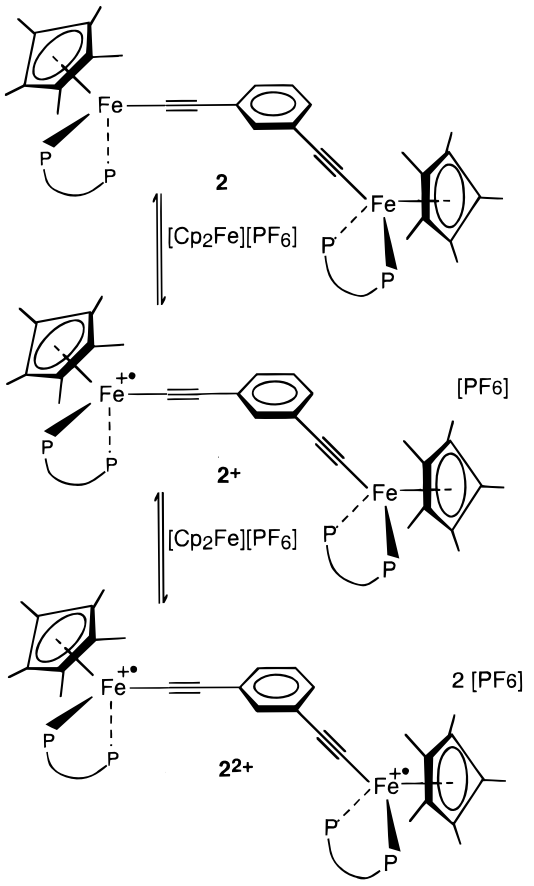

3. X-ray Crystal Structure of the Mixed-Valence Complexes [{Cp*(dppe)Fe(CC−)}$_2$(1,3-C$_6$H$_4$)][PF$_6$] ($\mathbf{2}^+$). Very few binuclear complexes with the general structure $M{-}C{\equiv}C{-}Ar{-}C{\equiv}C{-}M$ have been structurally characterized to date, and for all of them the two metal centers are in the same oxidation states.[26−29] The molecular structure of the trinuclear complex **3** was determined previously,[1] but despite numerous efforts, it was not possible to grow single crystals of the MV complexes $\mathbf{3}^+$ or $\mathbf{3}^{2+}$. On the other hand, single crystals of the MV $\mathbf{2}^+$ were obtained by slow diffusion of pentane into a CH_2Cl_2 solution, and the crystal structure was determined. Crystal data and refinement details are summarized in Table 2, and selected bond distances and bond angles are collected in Table 3. The molecular structure of the binuclear complex $\mathbf{2}^+$ is shown in Figure 1.

Complex $\mathbf{2}^+$ crystallizes in the triclinic space group $P\bar{1}$ with two molecules of methylene dichloride per unit cell. The hexafluorophosphate anion was found disordered between two positions with an occupancy ratio of 80:20. Similar arrangements of hexafluorophosphate

(23) Patoux, C.; Coudret, C.; Launay, J.-P.; Joachim, C.; Gourdon, A. *Inorg. Chem.* **1997**, *36*, 5037.
(24) Colbert, M. C. B.; Lewis, J.; Long, N. J.; Raithby, P. R.; Younus, M.; White, A. J. P.; Williams, D. J.; Payne, N. N.; Yellowlees, L.; Beljonne, D.; Chawdhury, N.; Friend, R. H. *Organometallics* **1998**, *17*, 3034.
(25) Long, N. J.; Martin, A. J.; Fabrizi de Biani, F.; Zanello, P. *J. Chem. Soc., Dalton Trans.* **1998**, 2017.
(26) Paul, F.; Lapinte, C. *Coord. Chem. Rev.* **1998**, *178−180*, 427.
(27) Behrens, U.; Hoffmann, K.; Kopf, J.; Moritz, J. *J. Organomet. Chem.* **1976**, *117*, 91
(28) Fyfe, H. B.; Mlekuz, M.; Zargarian, D.; Taylor, N. J.; Marder, T. B. *J. Chem. Soc., Chem. Commun.* **1991**, 188.
(29) Lewis, J.; Long, N. J.; Raithby, P. R.; Shields, G. P.; Wong, W.-Y.; Younus, M. *J. Chem. Soc., Dalton Trans.* **1997**, 4283.

Scheme 3

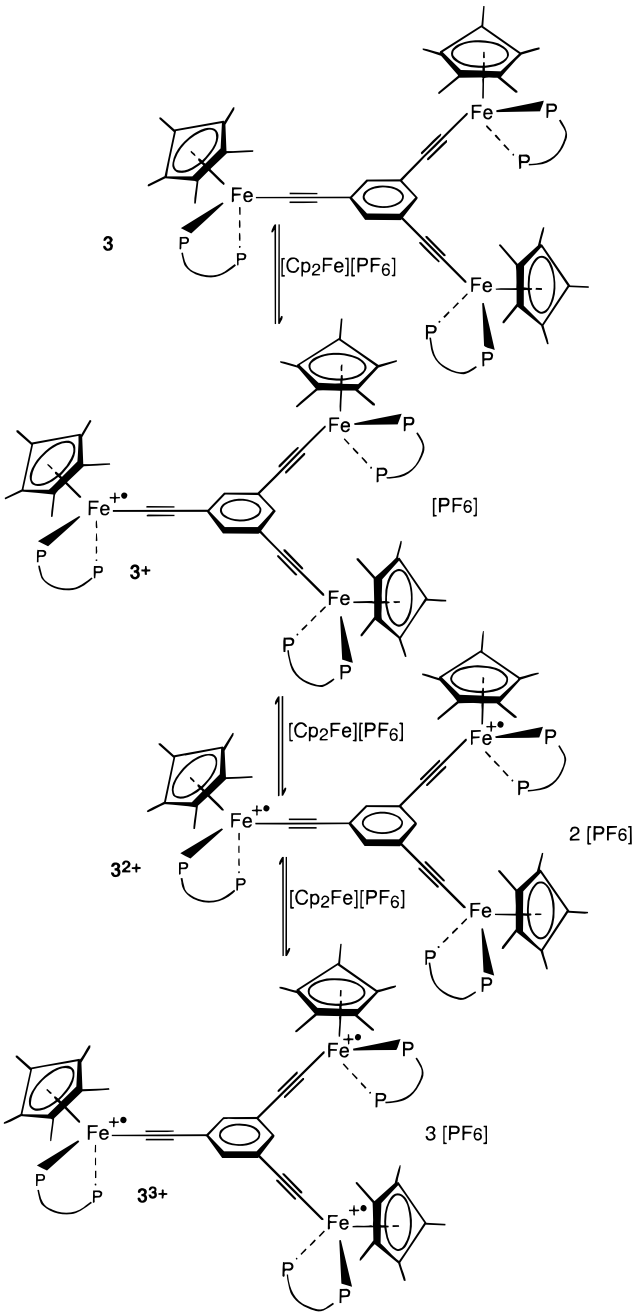

anions have already been observed in other mixed-valence compounds.[30] The bond distances and bond angles of the two Cp*Fe(dppe) units in the cation are rather close to each other and compare well with the data obtained for the trinuclear iron(II) complex **3**[1] and other related mononuclear iron(II) and iron(III) derivatives of the series.[26] The Fe−centroid distance for the Fe2 site is slightly larger than that for Fe1, suggesting that the Fe2 site is the Fe(III) center in the MV cation. Moreover, the averaged Fe−P distance for Fe2 is also marginally larger than that of Fe1, in agreement with the Fe(III) character of the Fe2 center. The assignment of the valence state is also confirmed by the positioning of the PF_6^- anion relative to the nearest metal center. Considering the two locations for the counteranion and their mean occupancies, the Fe1−P_{anion} and Fe2−P_{anion} distances are 15.40 and 8.15 Å, respectively. Thus, in the environment of the two iron centers of the cation, the electrostatic fields are not equivalent and would lead to an energy difference between the Fe_a(II)−Fe_b(III) and Fe_a(III)−Fe_b(II) vibronic states of the MV in the solid state. However, the very similar geometry of both iron centers should be associated with a weak energy of reorganization for the intramolecular electron transfer.

(30) Webb, R. J.; Geib, S. J.; Staley, D. L.; Rheingold, A. L.; Hendrickson, D. N. *J. Am. Chem. Soc.* **1990**, *112*, 5031.

Table 2. Experimental Crystallographic Data for 2^+

formula	$C_{82}H_{82}Fe_2P_5F_6$:2 CH_2Cl_2
fw	1617.88
cryst syst	triclinic
space group	$P\bar{1}$
a, Å	15.599(5)
b, Å	17.289(4)
c, Å	17.655(9)
α, deg	117.67(3)
β, deg	99.09(3)
γ, deg	96.87(2)
V, Å^3	4061(3)
Z	2
D_{calcd}, g/cm^3	1.323
F(000)	1678
μ(Mo Kα), cm^{-1}	5.73
T, K	293(2)
cryst size, mm	0.45 × 0.45 × 0.35
θ range for data collection, deg	1.34−24.97
variance of standards	0.2%
range of *hkl*	0.18; −20, +20; −20, +20
no. of reflns measd	14 852
no. of reflns obsd ($I>2\sigma(I)$)	5114
no. of data/restraints/params	14 274/0/871
R	0.0978
R_w[a]	0.27
S_w	0.977
residual density e Å^{-3}, $\Delta\rho$	1.05

Table 3. Selected Bond Distances (Å) and Angles (deg) for 2^+

Fe(1)−P(1)	2.213(4)	C(39)−C(40)	1.364(16)
Fe(1)−P(2)	2.248(5)	C(40)−C(81)	1.374(17)
Fe(2)−P(3)	2.233(3)	C(80)−C(81)	1.419(15)
Fe(2)−P(4)	2.275(4)	C(79)−C(80)	1.418(16)
Fe(1)−C(37)	1.877(13)	C(79)−C(82)	1.378(15)
Fe(2)−C(77)	1.880(11)		
C(37)−C(38)	1.204(15)	Fe(1)−$Cp^*_{(centroid)}$	1.731
C(77)−C(78)	1.193(14)	Fe(2)−$Cp^*_{(centroid)}$	1.771
C(38)−C(39)	1.424(16)	Fe(1)−Fe(2)	10.247
C(78)−C(79)	1.451(14)		
P(1)−Fe(1)−P(2)	85.12(14)		
P(3)−Fe(2)−P(4)	84.31(13)	Fe(1)−C(37)−C(38)	177.9(10)
		Fe(2)−C(77)−C(78)	178.3(11)
P(1)−Fe(1)−C(37)	83.4(3)		
P(2)−Fe(1)−C(37)	87.3(4)	C(37)−C(38)−C(39)	173.0(12)
P(3)−Fe(2)−C(77)	82.8(3)	C(77)−C(78)−C(79)	175.2(11)
P(4)−Fe(2)−C(77)	87.8(4)		

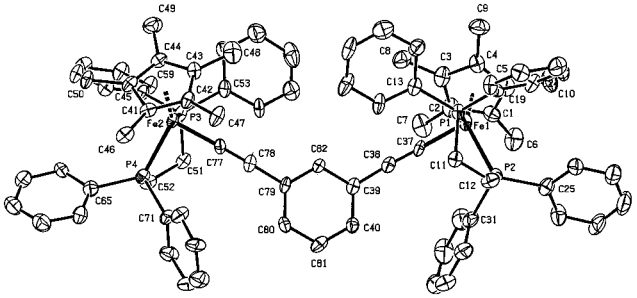

Figure 1. X-ray structure of the complex [{Cp*(dppe)Fe-(C≡C−)}$_2$(1,3-C_6H_4)][PF_6] (**2**$^+$) (view perpendicular to the plane of the central phenyl ring).

Table 4. IR $\nu_{C\equiv C}$ Bond Stretching and Mössbauer Parameters for the Mono-, Bi-, and Trinuclear Fe(II) and Fe(III) Complexes

		Mössbauer (mm s^{-1} vs Fe, 80 K)				
		Fe(II)		Fe(III)		
compd	IR (cm^{-1}) in CH_2Cl_2	IS	QS	IS	QS	%[a]
1	2049	0.27[b]	2.00[b]			100/0
$\mathbf{1}^+$	2022			0.27[a]	0.90	0/100
2	2049	0.20[b]	2.00[b]			100/0
$\mathbf{2}^+$	2044/1998	0.25	2.00	0.25	0.85	50/50
$\mathbf{2}^{2+}$	2006			0.28	0.89	0/100
3	2050	0.26[b]	1.99[b]			100/0
$\mathbf{3}^+$	2044/1990	0.25	1.99	0.24	0.95	66/34
$\mathbf{3}^{2+}$	2041/2010	0.19	1.71	0.24	0.95	34/66
$\mathbf{3}^{3+}$	2011			0.28	0.88	0/100

[a] Relative spectral absorption areas of the Mössbauer doublets. [b] From ref 1.

The bridging phenyl ring is essentially planar, and the deviation from coplanarity of the ethyndiyl spacer is significant (average 0.183 Å). The two iron atoms are positioned above and below the plane defined by the connecting arene with deviations of 0.38 and −0.42 Å. The planes defined by the two C_5 rings are almost perpendicular (91.3°). As usual, the two organoiron centers clearly adopt a pseudooctahedral geometry. Three coordination positions are occupied by the Cp* ring, whereas the two phosphorus atoms and the C_α carbon of the ethyndiyl fragments are positioned at the three remaining sites. In the limit of the structure determination, one notes that the Fe^2-C_α distance is longer than the Fe^1-C_α length, whereas the $C_\alpha-C_\beta$ triple bond length is shorter on the Fe^2 side. Comparison of the bond distances determined for $\mathbf{2}^+$ with those of the neutral complex **3** reveals that both iron building blocks have been affected by the one-electron oxidation. The variation of the $Fe-C_\alpha$ and $C_\alpha-C_\beta$ bond lengths, within the limit of the esd's, is not significant. However, the $Cp^*_{centroid}-Fe$ and Fe−P distances are roughly 0.01 Å shorter in the neutral complex than in the radical cation $\mathbf{2}^+$. These experimental data establish the electronic interaction between the two redox-active iron centers and are in agreement with the DF calculations (see section 9).

4. Infrared Spectroscopy. The IR spectra of the mono-, bi-, and trinuclear iron(II) and iron(III) complexes display a single $\nu_{(C\equiv C)}$ stretching band, as previously reported (see Table 4).[2] In the homovalent series, this vibration was observed at lower frequency for the Fe(III) compounds than for their Fe(II) precursors. Depending upon the number of metal sites, the decrease ranges from 27 to 44 cm^{-1}. This diminution was attributed to a weak contribution of an allenylidene-type resonance structure in the case of the iron(III) complexes (see Scheme 5 in ref 2). This means that upon one-electron oxidation of the metal centers, the C≡C bond lengths increase whereas the Fe−C bond distances decrease concomitantly. This trend has been found to agree with the DF calculations.[2]

In contrast, the IR spectra of the mixed-valence complexes $\mathbf{2}^+$, $\mathbf{3}^+$, and $\mathbf{3}^{2+}$ show two distinct $\nu_{(C\equiv C)}$ stretching bands. The vibration mode at higher frequency can be assigned to the $\nu_{(C\equiv C)}$ stretching mode of the Fe(II)−C≡C fragments, and the second absorption band corresponds to the Fe(III)−C≡C groups. Comparison of the IR data given in Table 4 indicates a weak interaction between the Cp*(dppe)Fe(C≡C)− building blocks through the arene connector. Indeed, the presence of the iron(III) center in the *meta* position with respect to the iron(II) group lowers the frequencies of the C≡C triple bond stretching mode on the iron(II) side by 5, 6, and 9 cm^{-1} for $\mathbf{2}^+$, $\mathbf{3}^+$, and $\mathbf{3}^{2+}$, respectively. Interestingly, a shift to lower wavenumbers is also observed for the Fe(III)(C≡C) groups. Relative to the corresponding homovalent iron(III) complex the decrease of the wavenumbers are 8 and 21 cm^{-1} for the complexes $\mathbf{2}^+$ and $\mathbf{3}^+$, respectively.

The IR data suggest that the weight of cumulenic limiting resonant structures should be higher in the mixed-valence systems with only one unpaired electron than in the pure iron(III) binuclear or trinuclear derivatives. Indeed, it is possible that an allenylidene-like structure with the cationic charge localized on one iron center and the radical delocalized on the arene ring contributes to stabilization of the mixed-valent state. Such a limiting structure is in full agreement with the DF calculations (see section 9), which also shows that the spin density on the connecting arene is higher in MV $\mathbf{2}^+$ than in the homovalent derivative $\mathbf{2}^{2+}$. In the case of the trinuclear complex with two unpaired electrons, $\mathbf{3}^{2+}$, the IR data indicate that the electronic structure of the Fe(III)(C≡C) fragments is the same as that of the homovalent $\mathbf{3}^{3+}$. This is also supported by the DF calculations. In this compound, only the Fe(II)-

Scheme 4

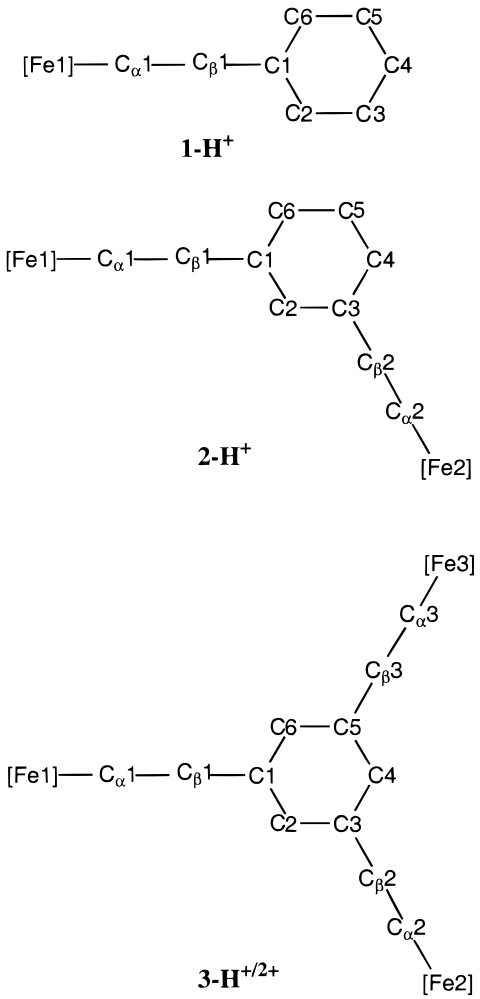

(C≡C) group seems to be concerned with the electronic reorganization. On the other hand, the presence of two distinct absorption bands for the C≡C bond stretching provides evidence for localized oxidation states. The intramolecular electron transfer from one iron center to the other is slow on the IR time scale. Accordingly, electron transfer from metal to metal takes place in CH_2Cl_2 solution and in solid state as well, with a rate constant $k_e < 10^{11}$ s^{-1}.[31]

5. Mössbauer Spectroscopy. The use of ^{57}Fe Mössbauer spectroscopy for the study of mixed-valence species is particularly interesting.[32−38] It gives precise information on the remote iron centers and allows determination of the oxidation states, estimation of the spin distribution between the remote ends and the organic bridge, and an evaluation of the electron-transfer rate relative to the acquisition time of the technique.[39] Indeed, for a bis-iron MV compound, the presence of two distinct doublets in the spectrum is diagnostic of a localized-valence state with a rate constant $k_e \leq 10^6$ s^{-1}, whereas observation of a single averaged doublet is diagnostic of an untrapped-valence state with $k_e > 10^9$ s^{-1}.[30]

The Mössbauer spectra of the MV compounds $\mathbf{2}^+$, $\mathbf{3}^+$, and $\mathbf{3}^{2+}$ were run at 77 K and least-squares fitted with Lorentzian line shapes.[40] The quadrupole splitting (QS) and isomer shift (IS) parameters are given in Table 4. The spectrum of the MV species $\mathbf{2}^+$ displays two well-separated doublets with relative spectral absorption areas in 1:1 ratio. The parameters are very close to those obtained for the homovalent species **2** and $\mathbf{2}^{2+}$, indicating the presence of distinct Fe(II) and Fe(III) sites in $\mathbf{2}^+$. From the comparison of the IS and QS parameters of $\mathbf{2}^+$ with those of **2** and $\mathbf{2}^{2+}$, it appears that the spin density is essentially localized on one metal site. Furthermore, the Mössbauer spectrum recorded at 293 K shows the same pattern. As a consequence, it can be concluded that electron transfer is slow on the Mössbauer time scale. Therefore, in the solid state, the rate constant for electron transfer from one metal site to the other is smaller than 10^6 s^{-1}.

Similarly, the Mössbauer spectra of $\mathbf{3}^+$ and $\mathbf{3}^{2+}$ exhibit two doublets with relative spectral absorption areas in 1:3 and 2:3 ratios, respectively, indicating that the two trinuclear complexes are also trapped MV systems on the Mössbauer time scale. In the case of the MV $\mathbf{3}^+$, the more intense doublet has parameters characteristic of a Cp*(dppe)Fe(II) site, whereas the parameters of the smaller doublet are typical of a Cp*(dppe)Fe(III) center. In the case of $\mathbf{3}^{2+}$ the reverse situation occurs. Note, however, that the isomeric shift and the quadrupole splitting parameters of the Fe(II) site are smaller in $\mathbf{3}^{2+}$ than in the complexes $\mathbf{2}^+$ and $\mathbf{3}^+$. In the case of $\mathbf{3}^{2+}$, the Mössbauer data suggest that the electronic density at the Fe(II) center is lowered by interaction with the two Fe(III) sites.

Table 5. ESR Data[a] for $\mathbf{2}^+$, $\mathbf{3}^+$, $\mathbf{3}^{2+}$, and Related Compounds

X	g_{iso}	g_1	g_2	g_3	Δg	ref
$\mathbf{1}^{+b}$	2.156	1.975	2.033	2.460	0.485	2
$\mathbf{2}^+$	2.170	1.975	2.032	2.505	0.530	this work
$\mathbf{3}^+$	2.155	1.982	2.034	2.450	0.468	this work
$\mathbf{3}^{2+c}$	2.139	1.978	2.030	2.409	0.431	this work
[Fe]−C$_4$−[Fe]	2.054	1.999	2.054	2.108	0.109	39

[a] At 77 K in $CH_2Cl_2/C_2H_4Cl_2$ (1:1) glass. [b] From ref X. [c] A $\Delta m_s = 2$ transition was also observed (see text).

6. ESR Measurements. The X-band ESR spectra were run at 77 K in a rigid glass ($CH_2Cl_2/C_2H_4Cl_2$, 1:1) for samples of $\mathbf{2}^+$, $\mathbf{3}^+$, and $\mathbf{3}^{2+}$. The spectra display three features corresponding to the three components of the g tensor as expected for d^5 low-spin iron(III) in pseudooctahedral geometry. The g values extracted from the spectra are collected in Table 5, together with some g values from the literature for related compounds containing the same Cp*Fe(dppe) fragment. The resolution of the spectra of the trinuclear complexes was good enough to allow the observation of the hyperfine coupling with the phosphorus nuclei. In both spectra, the g_1 tensor component was split into a triplet with hyperfine coupling constants a_1 of 13 and 15 G for $\mathbf{3}^+$ and $\mathbf{3}^{2+}$, respectively. This observation constitutes definitive evidence for trapped MV systems in a frozen glass on the ESR time scale. Moreover, for MV compounds of the biferrocenium series, it has been established that the anisotropy of the signal ($\Delta g = g_1 - g_3$) decreases as the rate of intramolecular electron transfer increases.[33,41] The anisotropy tensor Δg was used to determine whether the rate of the electron transfer is greater than the ESR time scale (10^{-9}−10^{-10} s). In the case of the MV complexes $\mathbf{2}^+$, $\mathbf{3}^+$, and $\mathbf{3}^{2+}$ Δg is very close to the value determined for the mononuclear complex [Cp*Fe(dppe)(C≡C−C$_6$H$_5$)][PF$_6$] ($\mathbf{1}^+$), which is in agreement with a slow electron exchange between the metal sites. Note, for example, that a much smaller Δg value was observed in the case of the strongly coupled MV complex [Cp*(dppe)Fe−C≡C−C≡C−Fe(dppe)Cp*][PF$_6$] (**8**).[42]

The ESR spectrum of the tris(iron) biradical $\mathbf{3}^{2+}$ also exhibits a weak, but clearly resolved, signal at $g = 4.64$ due to the $\Delta m_s = 2$ transition characteristic of the triplet state ($S = 1$) of the ESR active species as expected for a diradical with two $S = 1/2$ spin carriers. The spectrum of $\mathbf{3}^{2+}$ is much more intense than that previously observed for the triradical $\mathbf{3}^{3+}$. Both spectra also differ in shape and position of the signals. Thus, the signal observed at half-field can be confidently attributed to MV $\mathbf{3}^{2+}$ and not to the amount of $\mathbf{3}^{3+}$ formed by comproportionation of the MV derivative. ESR spec-

(31) Ito, T.; Hamaguschi, T.; Nagino, H.; Yamaguschi, T.; Kido, H.; Zavarine, I. S.; Richmond, T.; Washington, J.; Kubiak, C. P. *J. Am. Chem. Soc.* **1999**, *121*, 4625.
(32) Greenwood, N. N. *Mössbauer Spectroscopy*; Chapman and Hall: London, 1971.
(33) Dong, T.-Y.; Hendrickson, D.; Pierpont, C. G.; Moore, M. F. *J. Am. Chem. Soc.* **1986**, *108*, 963.
(34) Moore, M. F.; Wilson, S. R.; Cohn, M. J.; Dong, T. Y.; Kampara, T.; Hendrickson, D. N. *Inorg. Chem.* **1985**, *24*, 4559.
(35) Dong, T.-Y.; Kampara, T.; Hendrickson, D. N. *J. Am. Chem. Soc.* **1986**, *108*, 5857.
(36) Kampara, T.; Hendrickson, D. N.; Dong, T.-Y.; Cohn, M. J. *J. Chem. Phys.* **1987**, *86*, 2362.
(37) Le Vanda, C.; Cowan, D. O.; Leitch, C.; Bechgaard, K. *J. Am. Chem. Soc.* **1974**, *96*, 6788.
(38) Le Vanda, C.; Bechgaard, K.; Cowan, D. O. *J. Org. Chem.* **1976**, *41*, 2700.
(39) Gütlich, P.; Link, R.; Trautwein, A. *Mössbauer Spectroscopy and Transition Metal Chemistry*; Springer-Verlag: Berlin, 1978; Vol. 3.
(40) Varret, F.; Mariot, J.-P.; Hamon, J.-R.; Astruc, D. *Hyperfine Interact.* **1988**, *39*, 67.
(41) Dong, T.-Y.; Sohel, C.-C.; Hwang, M.-Y.; Lee, T. Y.; Yeh, S.-K.; Wen, Y.-S. *Organometallics* **1992**, *11*, 573.
(42) Le Narvor, N.; Toupet, L.; Lapinte, C. *J. Am. Chem. Soc.* **1995**, *117*, 7129.

Table 6. Wavelength in nm (molar extinction coefficient, mol^{-1} cm^{-1}) of the UV−Vis Transitions[a] for 2^+, 3^+, and 3^{2+}

compd	$\pi \rightarrow \pi^*$	MLCT	LMCT
2	254 (28 000)	349 (15 000)	
$\mathbf{2}^+$	264 (47 000)	319 (17 000)	560 (2600), 650 (4000)
$\mathbf{2}^{2+}$	285 (57 000)		574 (4500), 662 (5500)
3	283 (53 000)	351 (35 000)	
$\mathbf{3}^+$	282 (49 000)	366 (22 000)	600 (2300), 710 (4400)
$\mathbf{3}^{2+}$	288 (56 000)		590 (4100), 688 (5500)
$\mathbf{3}^{3+}$	288 (56 000)		573 (5500), 662 (5500)

[a] At 77 K in CH_2Cl_2. For the MV complexes, the molar extinction coefficients were corrected to take into account the molar fraction of the components in solution.

troscopy establishes that the triplet state of the biradical $\mathbf{3}^{2+}$ is significantly populated at 77 K. As we have shown in a previous paper,[2] *meta* connections of the spin carriers around the central phenylene ring favor the triplet-ground-state configuration.[2] As a consequence, at high temperature, the singlet and triplet spin isomers are expected to be present simultaneously. Assuming that the magnetic interaction in the biradical trinuclear complex $\mathbf{3}^{2+}$ is not very different from that determined in the biradical dinuclear compound $\mathbf{2}^{2+}$ ($2J = 130.6$ cm^{-1}), the singlet/triplet population ratio at 293 K can be estimated close to the high-temperature limiting value of 25/75. This assumption is fully supported by the DF calculations (vide infra).

7. UV−Visible Spectroscopy. The UV spectra of all the binuclear and trinuclear complexes display intense absorption bands in the range 250−290 nm (Table 6). These high-energy transitions can be safely ascribed to ligand-centered (LC) $\pi-\pi^*$ electronic transition. The stepwise oxidation of the metal centers produces a shift of the band toward the near-UV, which indicates either stabilization of the empty ligand-based orbitals (π^*) or a destabilization of the occupied orbitals (π) upon oxidation. A second broad band is observed around 400 nm, which may be composed of several overlapping absorptions, as suggested by the presence of poorly solved shoulders. This band is responsible for the orange color of the neutral compounds **2** and **3**, but also exists in the deeply colored oxidized forms. These absorptions were assigned to metal-to-ligand charge-transfer (MLCT) processes, since such transitions are usually observed for related complexes.[43,44] The spectra of the oxidized $\mathbf{2}^+$, $\mathbf{2}^{2+}$, $\mathbf{3}^+$, $\mathbf{3}^{2+}$, and $\mathbf{3}^{3+}$ complexes present two transitions above 550 nm. Despite their weaker intensities, these transitions explain the dark green or blue colors of these salts in solution. They may be ascribed to ligand-to-metal charge transfer (LMCT) transitions. Such transitions are likely to take place after creation of an electronic vacancy in the HOMO after the oxidation (SOMO).[2,44]

8. Intervalence Bands and Experimental Electronic Couplings. The electronic coupling parameter V_{ab} (also denoted H_{ab})[4] can be calculated using the characteristics of the intervalence charge transfer (ICT) band. For such an experimental determination, one has to be able to observe clearly the ICT band(s), which can be masked or enhanced by other electronic transitions.[45] Bands were found in the near-IR region for the three MV compounds $\mathbf{2}^+$, $\mathbf{3}^+$, and $\mathbf{3}^{2+}$ (Figures 2−4). These bands, located in the tail of the LMCT transitions observed in the visible, are broad, and their maximum intensity is around 500 M^{-1} cm^{-1}. The position of ν_{max} depends only weakly on the solvent used. Thus, the increase of ν_{max} is less than 90 cm^{-1} when CH_2Cl_2 is replaced by either acetonitrile or methanol.

The spectra of the neutral complexes **2** and **3** do not contain any absorptions in the NIR range, but the spectrum of the homovalent Fe(III) radical cations $\mathbf{2}^{2+}$ and $\mathbf{3}^{3+}$ as well as $\mathbf{1}^+$ contain very weak absorptions around 5400 cm^{-1} (Table 7). These absorptions have

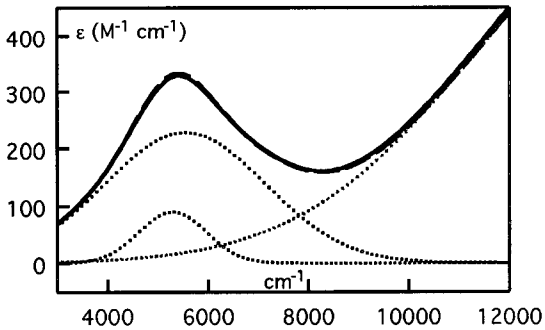

Figure 2. Experimental NIR absorption spectrum data for $\mathbf{2}^+$ in CH_2Cl_2 (solid line) and the deconvoluted ICT bands (dashed lines). The dashed line corresponds to the sum of the deconvoluted bands.

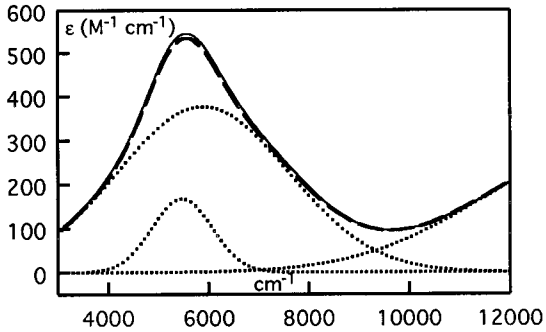

Figure 3. Experimental NIR absorption spectrum data for $\mathbf{3}^+$ in CH_2Cl_2 (solid line) and the deconvoluted ICT bands (dashed lines). The dashed line corresponds to the sum of the deconvoluted bands.

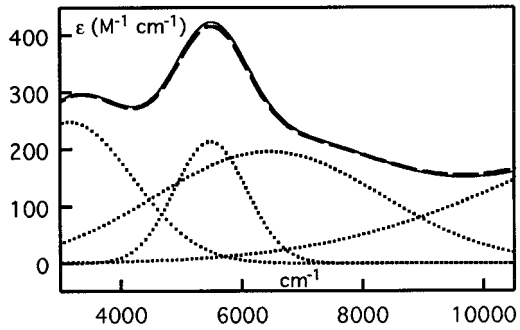

Figure 4. Experimental NIR absorption spectrum data for $\mathbf{3}^{2+}$ in CH_2Cl_2 (solid line) and the deconvoluted ICT bands (dashed lines). The dashed line corresponds to the sum of the deconvoluted bands.

(43) Wu, I. Y.; Lin, J. T.; Luo, J.; Sun, S.-S.; Li, C.-S.; Lin, K. J.; Tsai, C.; Hsu, C.-C.; Lin, J.-L. *Organometallics* **1997**, *16*, 2038.

(44) Le Stang, S.; Paul, F.; Lapinte, C. *Inorg. Chim. Acta* **1999**, *291*, 403.

(45) Ribou, A.-C.; Launay, J.-P.; Takahashi, K.; Nihara, T.; Tarutani, S.; Spangler, C. W. *Inorg. Chem.* **1994**, *33*, 1325.

Table 7. NIR Spectral Data for the Fe(III) Centers[a]

compd	ν_{max} (cm^{-1})	ϵ (M^{-1} cm^{-1})	$\Delta\nu_{1/2}$ (cm^{-1})
$\mathbf{1}^{+b}$	5465	90	1450
$\mathbf{2}^{+c,d}$	5290	90	1450
$\mathbf{2}^{2+b}$	5460	100	1600
$\mathbf{3}^{+c,d}$	5470	120	1450
$\mathbf{3}^{2+c,d}$	5480	200	1400

[a] CH_2Cl_2, 20 °C. [b] Direct measurements. [c] Obtained by deconvolution of the NIR spectrum. [d] The molar extinction coefficients were corrected to take into account the molar fraction of the components in solution.

weak intensity ($\epsilon \approx 150$ M^{-1} cm^{-1}) and correspond to a forbidden ligand field (LF) transition specific to the Cp*(dppe)Fe(III) fragment. Similar absorption bands were also found for Cp*(dppe)Fe(III)(C≡C−C_5H_4N)[44] complexes and related chromium radicals.[46] In many cases, this iron(III) contribution is too weak to significantly affect the intense ICT band of the Fe(II)−Fe(III) mixed-valence compounds previously studied in this series,[42,47,48] but in the present case, the intensity of the ICT band is also weak and the contribution of the LF transition must be considered.

Assuming that the ICT bands have Gaussian profiles, the spectra of the MV derivatives were deconvoluted in the range 3500−12 000 cm^{-1}.[49] As shown in Figures 2−4, results show good agreement between the sum of the spectral components and the experimental spectra after filtration of noise and residual vibrations due to the solvent subtraction. For the two $S = 1/2$ MV complexes $\mathbf{2}^+$ and $\mathbf{3}^+$, the band shape analysis reveals the presence of two absorption bands in addition to the tail of the MLCT bands. The parameters of the narrower band are similar to those of LF transition observed in the NIR spectra of the mononuclear complex $\mathbf{1}^+$ and the binuclear homovalent iron(III) compounds $\mathbf{2}^{2+}$ and $\mathbf{3}^{3+}$ (see Table 7). Therefore, it is unlikely that this band corresponds to an Fe(II) → Fe(III) ICT transition. The second component of the spectrum located at slightly higher energy is characteristic of an ICT band for a weakly coupled MV system. Indeed, the full width at half-height ($\Delta\nu_{1/2}$) of the band is very close to the theoretical value derived from the near-IR band position ν_{max} according to Hush's relationship for symmetrical MV complexes (see Table 8).[50] For the trinuclear mixed-valence compound $\mathbf{3}^{2+}$, which possesses two unpaired electrons, deconvolution of the experimental spectrum gives three Gaussian bands. One of those is characteristic of the LF transition (Table 7), and the two others are characteristic of metal-to-metal ICT transitions (Table 8).[51] This time again, the experimental parameters $\Delta\nu_{1/2}$ of the two ICT bands are close to the values expected from Hush's theory. Thus, according to the IR, Mössbauer, ESR, and NIR data, the iron centers are weakly coupled and these MV salts can be classified as class II MV complexes in the classification of Robin and Day.[6] Note that in this respect the weak solvent dependence of the ICT band is surprising. Indeed, solvent dependence of the ICT band for class II derivatives is usually large,[52,53] shifts of more than 1000 cm^{-1} having been reported.[50] In our series, the poor sensitivity of the MV species to the polarity of the solvent could result from a weak and similar solvation of the iron(II) and iron(III) centers. Such behavior also suggests that the energy of reorganization associated with the electron transfer should be rather low (see DF calculations).

Considering that the ICT bands fit with Gaussian band shapes, the electronic coupling parameters (V_{ab}, cm^{-1}) were calculated using the formula derived from Hush's theory for the binuclear MV complex $\mathbf{2}^+$ (eq 4, Table 8):[8,54]

$$V_{ab} = (2.06 \times 10^{-2})\frac{\sqrt{\bar{\nu}_{max}\epsilon_{max}\bar{\nu}_{1/2}}}{\Delta\mu/e} \qquad (4)$$

where ν_{max}, ϵ_{max}, and $\nu_{1/2}$ are the peak location, extinction coefficient, and full width at half-maximum, respectively. The term $\Delta\mu$ is the change in dipole moment between the ground and excited state and defines the effective charge-transfer distance, d_{ab} (Å) = $\Delta\mu/e$, where e is the unit charge. In the absence of direct measurement of $\Delta\mu$ by Stark spectroscopy for example, the through-space metal−metal separation has typically been used as the best estimate of d_{ab}.[55,56] The electronic coupling (V_{ab} = 0.020 eV) obtained for $\mathbf{2}^+$ is similar to the value reported for a diferrocenylbenzene MV complex with a *meta* connection of the cyclopentadienyl rings around the central arene.[23] Considering that the difference of potentials of the redox processes is larger for $\mathbf{2}^+$ than in the diferrocenylbenzene series (0.125 vs 0.090 V), the value of V_{ab} obtained for $\mathbf{2}^+$ is not as large as expected. As has been previously stated, the difference could arise from the actual charge-transfer distance d_{ab}, which is somewhat smaller than the distance between the metal ions.[57]

In the case of the trinuclear complex $\mathbf{3}^+$, one electron exchanges between three equivalent redox sites separated by nanoscale distances. Assuming that the three sites behave independently, the effective electronic coupling between the iron sites can be determined using the modified Hush's equation reported by Bonvoisin and Launay (eq 5, Table 8).[9] Equation 5 differs from eq 4 established for binuclear system by a factor of $\sqrt{2}$ in the denominator to take into account three equivalent redox centers. In agreement with this model a single ICT band is observed in the spectrum.

$$V_{ab} = (2.06 \times 10^{-2})\frac{\sqrt{\bar{\nu}_{max}\epsilon_{max}\bar{\nu}_{1/2}}}{d_{ab}\sqrt{2}} \qquad (5)$$

In the limits of accuracy of the measurements, the electronic coupling between the redox centers in the

(46) Atwood, C. G.; Geiger, W. E. *J. Am. Chem. Soc.* **1994**, *116*, 10849.
(47) Coat, F.; Lapinte, C. *Organometallics* **1996**, *15*, 477.
(48) Guillemot, M.; Toupet, L.; Lapinte, C. *Organometallics* **1998**, *17*, 1928.
(49) Reimers, J. R.; Hush, N. S. *Inorg. Chem.* **1990**, *29*, 4510.
(50) Hush criteria of the solvent dependence of the NIR intervalence band maximum used to distinguish class II and class III MV compounds fail in this case.
(51) Nelsen, S. F. *Chem. Eur. J.* **2000**, *6*, 581.
(52) Creutz, C.; Taube, H. *J. Am. Chem. Soc.* **1969**, *91*, 3988.
(53) Callahan, R. W.; Brown, G. M.; Meyer, T. J. *J. Am. Chem. Soc.* **1974**, *96*, 7827.
(54) Crutchley, R. J. *Adv. Inorg. Chem.* **1994**, *41*, 273.
(55) Bublitz, G. U.; Laidlaw, W. M.; Denning, R. G.; Boxer, S. G. *J. Am. Chem. Soc.* **1998**, *120*, 6068.
(56) Karki, L.; Hupp, J. T. *J. Am. Chem. Soc.* **1997**, *119*, 4070.
(57) Dong, Y.; Hupp, J. T. *Inorg. Chem.* **1991**, *31*, 3170.

Table 8. Spectroscopic Data Measured in CH_2Cl_2 (energy, extinction coefficient, and width of the intervalence transition) and Experimental and Theoretical V_{ab} Couplings

compd	ν_{max}, cm^{-1}	$\Delta\nu_{1/2}$(exp), cm^{-1}	$\Delta\nu_{1/2}$(calcd),[b] cm^{-1}	ϵ_{max},[a] $M^{-1}\,cm^{-1}$	d,[c] Å	V_{ab}(exp), cm^{-1}
$\mathbf{2}^+$	5540 ± 50	3700 ± 100	3600 ± 50	310	10.2	161 ± 2[d]
$\mathbf{3}^+$	5890 ± 50	3900 ± 100	3700 ± 50	440	10.2	143 ± 2[e]
$\mathbf{3}^{2+}$	6450 ± 50	4200 ± 100	3900 ± 50	250[f]	10.2	117 ± 2[ef]
	3150 ± 50	2500 ± 100	2700 ± 50	310[f]	10.2	71 ± 2[ef]

[a] Corrected values according to eqs 1−3 and Table 1. [b] For a class II compound $\Delta\nu_{1/2}(cm^{-1}) = \sqrt{2310\nu_{max}}$. [c] From X-ray data determined for $\mathbf{2}^+$. [d] Calculated using eq 4. [e] Calculated using eq 5. [f] Determined assuming a unique species $\mathbf{3}^{2+}$; in the absence of assignment of the ICT bands to the triplet and singlet states, the calculation of the electronic coupling for these two discret species cannot be carried out.

trinuclear complex $\mathbf{3}^+$ is the same as in the binuclear $\mathbf{2}^+$. A similar observation was previously made by comparison of two- and three-redox-center MV organic compounds.[9,10] The authors concluded that one cannot easily distinguish between a case where one electron moves toward one hole and the case where one electron moves toward two holes using the ICT bands. This applies also for organometallic systems.

In the case of the diradical $\mathbf{3}^{2+}$ the situation is quite different. The two $S = 1/2$ centers do not behave independently, since there is a magnetic exchange interaction between the unpaired electrons. At 20 °C, both singlet and triplet states are populated and the relative population ratio can be estimated close to the high-temperature limit (e.g., 25/75; see the ESR section). As depicted in Scheme 1 and discussed in the Introduction, one electron of the site c can move to either of the sites a or b. Different electron-transfer pathways are expected to occur in the singlet and triplet states (i.e., $Vac_T = Vbc_T \neq Vac_S = Vbc_S$). This assumption is supported by the presence of two distinct NIR bands in the spectrum of $\mathbf{3}^{2+}$ (Figure 4). To the best of our knowledge, this observation constitutes the first experimental support for the existence of two independent pathways for electron transfer in the singlet and triplet states of a synthetic MV system. In comparison with $\mathbf{3}^+$, one of the ICT bands of $\mathbf{3}^{2+}$ is located at lower energy, whereas the second one is observed at higher energy. Therefore, with respect to the case of independent sites, it seems that the magnetic exchange interactions would either increase or decrease the adiabaticity of the electron-transfer process, depending on the parallel or antiparallel orientation of the unpaired spins. However, the assignment to singlet and triplet states of the ICT bands observed in the NIR spectrum of $\mathbf{3}^{2+}$ cannot be done either on the basis of the experimental data or deduced from the results of the DF calculations. Consequently, accurate determination of the respective molar absorption coefficients and electronic couplings cannot be calculated. Further work including variable-temperature NIR spectroscopy will be carried out in our group to understand the mutual interactions between the magnetic and electronic couplings.

In these symmetrical charge-localized intervalence compounds, besides the electronic coupling (V_{ab}), the vertical reorganization energy (λ) constitutes a second fundamental parameter.[4] In the Marcus−Hush model, the diabatic energy surfaces are parabolas and their energy separation at the ground state is λ, which is the transition energy of the ICT band at its maximum ($\lambda = h\nu_{max}$).[58] Considering the *meta*-phenylene topology of the complexes $\mathbf{2}^+$ and $\mathbf{3}^+$, the reorganization energy associated with electron transfer in these compounds is quite low ($\lambda \approx 5540$ and 5890 cm^{-1}, respectively). Indeed, for compounds with the same topology much larger values have been reported (~7000 cm^{-1} for purely organic systems[9] and ~8500 cm^{-1} in the case of organometallic compounds[23]). As a consequence, the diabatic energy surfaces corresponding to the MV complexes $\mathbf{2}^+$ and $\mathbf{3}^+$ are flattened and the activation free energy for the thermal electron-transfer barrier ΔG^* given by eq 6 is small (3.5 kcal mol^{-1}).[51]

$$\Delta G^*(cm^{-1}) = \left(\frac{\lambda}{4} - V_{ab}\right) + V_{ab}{}^2/\lambda \qquad (6)$$

In the case of the MV $\mathbf{3}^{2+}$ the assignment of the NIR bands to singlet and triplet cannot be done on the basis of either our results or the literature data.

9. Theoretical Calculations. Spin-unrestricted density functional (DF) molecular-orbital calculations were performed in order to provide the electronic structure of the mixed-valence systems $\mathbf{2}^+$ and $\mathbf{3}^{+/2+}$ (see the Experimental Section for computational details). These systems were modeled by $[\{Fe(Cp)(PH_3)_2(C{\equiv}C-)\}_2(1,3\text{-}C_6H_4)]^+$ ($\mathbf{2\text{-}H}^+$) and $[\{Fe(Cp)(PH_3)_2(C{\equiv}C-)\}_3(1,3,5\text{-}C_6H_3)]^{+/2+}$ ($\mathbf{3\text{-}H}^{+/2+}$), respectively, to reduce computational effort. Results on the cationic model $[Fe(Cp)(PH_3)_2(C{\equiv}C-C_6H_5)]^+$ ($\mathbf{1\text{-}H}^+$) are recalled for comparison.[1,2]

Geometry Optimizations. The results of partial geometry optimizations are given in Table 9 for the cationic species $\mathbf{2\text{-}H}^+$ and $\mathbf{3\text{-}H}^{+/2+}$ together with those published previously[2] for the related neutral and "fully" oxidized species in order to discuss the metrical changes upon oxidation. The X-ray data of $\mathbf{2}^+$ show a slight structural asymmetry (note however the rather high esd's), suggesting that this species is weakly valence-trapped, as supported by Mössbauer spectroscopy (vide supra). Consequently, calculations were carried out on both symmetrical and nonsymmetrical structural arrangements for $\mathbf{2\text{-}H}^+$ and $\mathbf{3\text{-}H}^{+/2+}$ in order to compare valence-delocalized geometries and presumably valence-localized geometries. The broken-symmetry formalism was used for the latter (see computational details).

The nodal properties of the HOMOs of the neutral species were described previously.[2] HOMOs in **2-H** result from antibonding interactions between dπ orbitals of the $Fe(Cp)(PH_3)_2$ fragments and out-of-plane π orbitals of the bis(ethynyl)benzene ligand. HOMOs in **3-H**

(58) Sanchez, F.; Perez-Tejeda, P.; Perez, F.; Lopez-Lopez, M. *J. Chem. Soc., Dalton Trans.* **1999**, 3035.

Table 9. Selected Optimized Bond Lengths (Å) and Bonding Energies (BE, eV) for the Complex Models $[Fe(Cp)(PH_3)_2(C{\equiv}C{-}C_6H_5)]^n$+ (1-H^{n+}) ($n$ = 0, 1), $[\{Fe(Cp)(PH_3)_2(C{\equiv}C{-})\}_2(1,3\text{-}C_6H_4)]^{n+}$ (2-H^{n+}) (n = 0, 1, 2), and $[\{Fe(Cp)(PH_3)_2(C{\equiv}C{-})\}_3(1,3,5\text{-}C_6H_3)]^{n+}$ (3-H^{n+}) (n = 0, 1, 2, 3)

	1-H	1-H$^+$	2-H	2-H$^+$	2-H$^+$ (BS)[a]	2-H^{2+} triplet	3-H	3-H$^+$	3-H$^+$ (BS)	3-H^{2+} singlet	3-H^{2+} triplet	3-H^{3+} quartet
BE	−182.07	−176.05	−289.71	−284.76	−284.75	−276.61	−397.26	−392.62	−392.63	−385.00	−385.15	−375.36
Fe1−C$_\alpha$1	1.901	1.847	1.879	1.860	1.873	1.842	1.893	1.876	1.872	1.831	1.865	1.861
Fe2−C$_\alpha$1			1.879	1.860	1.854	1.842	1.893	1.876	1.880	1.831	1.865	1.861
Fe3−C$_\alpha$1							1.893	1.876	1.863	1.831	1.865	1.861
C$_\alpha$1−C$_\beta$1	1.239	1.251	1.235	1.244	1.242	1.247	1.238	1.240	1.239	1.242	1.249	1.244
C$_\alpha$2−C$_\beta$2			1.235	1.244	1.244	1.247	1.238	1.240	1.239	1.242	1.249	1.244
C$_\alpha$3−C$_\beta$3							1.238	1.240	1.242	1.242	1.249	1.244
C$_\beta$1−C$_1$	1.434	1.414	1.423	1.415	1.418	1.415	1.430	1.425	1.421	1.408	1.424	1.426
C$_\beta$2−C$_3$			1.423	1.415	1.417	1.415	1.430	1.425	1.423	1.408	1.424	1.426
C$_\beta$3−C$_5$							1.430	1.425	1.423	1.408	1.424	1.426

[a] Broken symmetry.

Table 10. Energies (eV) and Percentage Compositions of the HOMO of the Cationic Complex Models $[\{Fe(Cp)(PH_3)_2(C{\equiv}C{-})\}_2(1,3\text{-}C_6H_4)]^+$ (2-H$^+$) and $[\{Fe(Cp)(PH_3)_2(C{\equiv}C{-})\}_3(1,3,5\text{-}C_6H_3)]^{+/2+}$ (3-H$^{+/2+}$)

					singlet	triplet	
	2-H$^+$	2-H$^+$ (BS)	3-H$^+$	3-H$^+$ (BS)[a]	3-H^{2+}	3-H^{2+}	
Occ (↑/↓)[b]	1/0	1/0	1/0	1/0	2/2	1/0	2/1
ϵ (eV) (↑/↓)	−6.92/−6.50	−6.92/ −6.60	−6.27/−5.93	−6.15/−5.94	−8.81/−8.81	−9.21/−8.51	−8.87/−8.64
Fe1 (↑/↓)	23.62/23.62	20.67/20.77	18.06/18.06	18.94/19.01	11.19/11.19	18.60/18.60	19.87/19.86
Fe2 (↑/↓)	23.62/23.62	21.73/21.84	18.06/18.06	18.95/19.06	11.19/11.19	18.60/18.60	19.87/19.86
Fe3 (↑/↓)			18.06/18.06	18.75/18.85	11.19/11.19	18.60/18.60	19.87/19.86
C$_{\alpha1}$ (↑/↓)	4.22/4.22	3.60/3.61	2.81/2.81	2.17/2.18	4.97/4.97	2.52/2.52	1.45/1.45
C$_{\alpha2}$ (↑/↓)	4.22/4.22	3.91/3.93	2.81/2.81	2.21/2.22	4.97/4.97	2.52/2.52	1.45/1.45
C$_{\alpha3}$ (↑/↓)			2.81/2.81	2.99/3.00	4.97/4.97	2.52/2.52	1.45/1.45
C$_{\beta1}$ (↑/↓)	9.60/9.60	8.16/8.20	7.34/7.34	7.60/7.64	5.57/5.57	7.09/7.09	7.20/7.22
C$_{\beta2}$ (↑/↓)	9.60/9.60	9.06/9.10	7.34/7.34	7.78/7.82	5.57/5.57	7.09/7.09	7.20/7.22
C$_{\beta3}$ (↑/↓)			7.34/7.34	7.91/7.96	5.57/5.57	7.09/7.09	7.20/7.22

[a] Broken symmetry. [b] Spin-up, spin-down.

mainly result from antibonding interactions between metal dπ orbitals of the Fe(Cp)(PH$_3$)$_2$ fragments and in-plane π/σ orbitals of the tris(ethynyl)benzene ligand. They are M−C$_\alpha$ antibonding, C$_\alpha$−C$_\beta$ bonding, and C$_\beta$−C(Ph) bonding in both cases. Consequently, a slight shortening of the optimized Fe−C$_\alpha$ and C$_\alpha$−C$_\beta$ distances and a slight lengthening of the optimized C$_\beta$−C(Ph) distances are oberved upon depopulation of these HOMOs (see Table 9). These metrical changes are in turn very weak because of the important delocalization of the HOMOs all over the molecules. As expected, metrical parameters for Fe−C$_\alpha$, C$_\alpha$−C$_\beta$, and C$_\beta$−C(Ph) are rather similar inside a series (neutral or cationic) and fall in the experimentally observed range of available values. More interestingly, a very weak asymmetry is computed for the broken-symmetry geometry of **2-H**$^+$ since the Fe−C$_\alpha$ separations differ slightly, by 0.019 Å (Fe1−C$_\alpha$1 = 1.873 and Fe2−C$_\alpha$2 = 1.854 Å, see Scheme 4 for atom numbering), in agreement with the crystallographic data for **2**$^+$. An even weaker asymmetry is computed for the broken-symmetry geometries of **3-H**$^+$ (Fe1−C$_\alpha$1 = 1.872, Fe2−C$_\alpha$2 = 1.880, and Fe3−C$_\alpha$3 = 1.863 Å). Broken-symmetry geometry optimization of **3-H**$^{2+}$ did not converge, preventing any comparison with full-symmetry structures of **3-H**$^{2+}$.

Electronic Structures. Surprisingly enough, at the level of accuracy of the method used, we can consider that in the case of **2-H**$^+$ and **3-H**$^+$ the full-symmetry and the broken-symmetry geometries are nearly isoenergetic (see Table 9), and their electronic structures are highly comparable. In the case of **3-H**$^{2+}$ the triplet state is slightly energetically favored over the singlet state (see Table 9), in agreement with the ESR measurements of **3**$^{2+}$.[60] Table 10 shows the composition of the HOMO for **2-H**$^+$, **3-H**$^+$, and **3-H**$^{2+}$ obtained from full- and broken-symmetry calculations. In all the broken-symmetry geometries, the HOMO is rather delocalized over the whole molecular backbone and nearly equally distributed on the metal atoms (ca. 20% each). It is closely similar to those computed for the full-symmetry geometries.

Net spin densities given in Table 11 for various cationic species indicate that the spin density is rather delocalized on the iron centers and to a lesser extent on the C$_\beta$ carbon atoms and carbon atoms of the phenyl ring in the case of the full-symmetry geometries. This spin density delocalization is retained upon reduction of symmetry since only a very weak asymmetry in the net spin densities is computed for the broken-symmetry geometries (the largest difference is computed for the iron spin densities which differ by 0.047 in **2-H**$^+$). It is noteworthy that in the case of **2-H**$^+$ the spin density distributed on the phenyl ring is larger than that computed for the "fully" oxidized model **2-H**$^{2+}$ (22.9 and 16.0% of the total spin density in **2-H**$^+$ and **2-H**$^{2+}$, respectively). On the other hand, a very small amount of spin density is computed on the phenyl ring in the

(59) Webb, R. J.; Dong, T.-Y.; Pierpont, C. P.; Boone, S. R.; Chadha, R. K.; Hendrickson, D. N. *J. Am. Chem. Soc.* **1991**, *113*, 4806.

(60) The computed energy difference between the singlet and triplet states of **3**$^{2+}$ is too large. DFT calculations do not reproduce well the energy of the singlet state of magnetic polynuclear compounds if the broken-symmetry (BS) formalism (allowing spin "localization") is not used (see for example: Bencini, A.; Gatteschi, D.; Totti, F.; Sanz, D. N.; McClaverty, J. A.; Ward, M. D. *J. Phys. Chem.* **1998**, *A102*, 10545). Nevertheless, since the BS geometry of **3**$^{2+}$ did not converge, the energy of the nonbroken-symmetry geometry ("delocalized" spins) was taken for the singlet state, to estimate the ground state of **3**$^{2+}$.

Table 11. Net Spin Densities Computed for the Cationic Complex Models $[Fe(Cp)(PH_3)_2(C{\equiv}C-)(1\text{-}C_6H_5)]^+$ (1-H$^+$), $[\{Fe(Cp)(PH_3)_2(C{\equiv}C-)\}_2(1,3\text{-}C_6H_4)]^+$ (2-H$^+$), and $[\{Fe(Cp)(PH_3)_2(C{\equiv}C-)\}_3(1,3,5\text{-}C_6H_3)]^{+/2+}$ (3-H$^{+/2+}$)

	1-H$^+$	2-H$^+$	2-H$^+$ (BS)[a]	3-H$^+$	3-H$^+$ (BS)	3-H^{2+} triplet
Fe1	0.602	0.291	0.274	0.248	0.246	0.528
Fe2		0.291	0.321	0.248	0.249	0.528
Fe3				0.248	0.248	0.528
C_α1	0.080	−0.003	−0.008	−0.004	−0.004	−0.053
C_α2		−0.003	0.002	−0.004	−0.004	−0.053
C_α3				−0.004	−0.004	−0.053
C_β1	0.193	0.116	0.102	0.100	0.102	0.213
C_β2		0.116	0.125	0.100	0.100	0.213
C_β3				0.100	0.097	0.213
C1	0.008	−0.029	−0.028	−0.008	−0.008	−0.019
C2	0.075	0.001	0.001	0.008	0.008	0.014
C3	−0.031	−0.029	−0.029	−0.008	−0.008	−0.019
C4	0.124	0.175	0.170	0.008	0.008	0.014
C5	−0.031	−0.057	−0.054	−0.008	−0.008	−0.019
C6	0.075	0.175	0.169	0.008	0.008	0.014

[a] Broken symmetry.

cases of **3-H**$^+$ and **3-H**$^{2+}$. Such results are in accord with the IR spectroscopy measurements (vide supra).

Conclusions

Results described above have clearly shown that the *meta* connection of Cp*Fe(dppe) units through the phenylethynyl rigid spacer leading to the formation of the organometallic mixed-valence **2**$^+$ and **3**$^{+/2+}$ allows electron transfer at nanoscale distances. Spectroscopic investigations provide evidence for localized oxidation states. Analyses of the NIR spectra show a single ICT band for the one-unpaired-electron systems **2**$^+$ and **3**$^+$. In these MV compounds a rather weak electronic coupling ($V_{ab} \approx 150$ cm^{-1}) is associated with a weak reorganization energy ($\lambda \approx 5500$ cm^{-1}) and a low barrier for the thermal process ($\Delta G^\ddagger < 4$ kcal mol^{-1}), which is far from usual in mixed-valence derivatives. The corresponding parabolic energy surfaces are supposed to be flattened. Such energy profiles are supported by DF results, which indicate that the total energy of the cationic species is almost independent of the geometry (symmetrical or nonsymmetrical). Indeed, DF calculations, which indicate that the cationic species **2-H**$^+$ and **3-H**$^{+/2+}$ are rather valence-delocalized species, show at first sight some apparent discrepancy with the experimental data. However, they were carried out on models in the "gas phase" in the absence of the electrostatic field of the counteranions which asymmetrically surround the cationic species **2**$^+$, for instance. The extreme environmental sensitivity of the rate of intramolecular electron transfer has been recognized for some MV complexes.[60] External factors such as asymmetric electrostatic field already mentioned, solvation, steric interaction, or structural distortion, which have not been taken into account in the calculations, must induce electronic localization in the mixed-valence species reported here. In the case of the trinuclear system **3**$^{2+}$, which behaves as a two-unpaired-electron system, deconvolution of the experimental NIR spectrum shows two ICT bands. This experimental observation supports the hypothesis of two independent ways to transfer electron in the singlet and triplet states of such a MV complex.

Experimental Section

General Data. All the manipulations were carried out under an argon atmosphere using Schlenk techniques or in a Jacomex 532 drybox filled with nitrogen. Routine NMR spectra were recorded using a Bruker DPX 200 spectrometer. High-field NMR spectra experiments were performed on a multinuclear Bruker WB 300 instrument. Chemical shifts are given in parts per million relative to tetramethylsilane (TMS) for ^{1}H and ^{13}C NMR spectra and H_3PO_4 for ^{31}P NMR spectra. X-Band ESR spectra were recorded on a Bruker ESP-300E spectrometer. An Air Products LTD-3-110 liquid helium transfer system was attached for the low-temperature measurements. The ^{57}Fe Mössbauer spectra were obtained by using a constant acceleration spectrometer previously described with a 50 mCi ^{57}Co source in a Rh matrix. The sample temperature was controlled by an Oxford MD306 cryostat and an Oxford ITC4 temperature controller. Computer fitting of the Mössbauer data to Lorenzian line shapes was carried out with a previously reported computer program. The isomer shift values are reported with respect to iron foil at 298 K and are not corrected for the temperature-dependent second-order Doppler shift. The Mössbauer sample cell consists of a 2 cm diameter cylindrical plexiglass holder. Elemental analyses were performed at the Centre de Microanalyses du CNRS, Lyon-Solaise, France. The syntheses of the compounds **1**, **1**$^+$, **2**, **2**$^{2+}$, **3**, **3**$^{3+}$, and **4** have been described elsewhere.[1,2]

Calculation of the Molar Fraction x^{n+}. Let us consider the equilibria eqs 2 and 3. The comproportionation constants are $K_{c1} = [x^+]^2/[x][x^{2+}]$ and $K_{c2} = [x^{2+}]^2/[x^+][x^{3+}]$. The conservation of masses and charges provides two other equations: $[x] + [x^+] + [x^{2+}] + [x^{3+}] = 1$ and $[x^+] + 2[x^{2+}] + 3[x^{3+}] = n$, n being the number of metal centers oxidized. The system of equations was solved for $K_{c1} = K_{c2} = 130$, $n = 1, 2$, by successive iterations using the Excel worksheet and a personal computer.

[{Cp*(dppe)Fe(CC−)}$_2$(1,3-C$_6$H$_4$)][PF$_6$] (2$^+$). To 0.190 g (0.15 mmol) of **2** in 30 mL of CH_2Cl_2 was added 0.047 g (0.95 equiv) of ferrocenium hexafluorophosphate. The initially orange solution turned rapidly olive green. The mixture was stirred for 5 h at room temperature and filtered before the solvent was removed under vacuum. The solid residue was washed with diethyl ether to extract ferrocene, and measurement of the yield of the latter allowed determination of the degree of completion of the reaction. The dark green powder was dried for 15 h under vacuum. Recrystallization at low temperature (−20 °C) from CH_2Cl_2/pentane (1:3) gave 0.206 g (93% yield) of **2**$^+$. Anal. Calcd for $C_{82}H_{82}F_6Fe_2P_5{\cdot}2/3CH_2Cl_2$: C, 62.39, H, 5.36. Found: C, 62.19, H, 5.30.

[{Cp*(dppe)Fe(CC−)}$_3$(1,3,5-C$_6$H$_3$)][PF$_6$] (3$^+$). A 0.225 g (0.12 mmol) sample of **3** in 30 mL of CH_2Cl_2 was added to 0.038 g (0.95 equiv) of ferricinium hexafluorophosphate. The initially orange solution turned rapidly to olive green. The mixture was stirred for 6 h at room temperature and filtered before the solvent was removed under vacuum. The solid residue was washed with diethyl ether (5 × 20 mL) to extract the ferrocene, and the measurement of the yield of the latter allowed a determination of the degree of completion of the reaction. The dark green powder was dried under vacuum. Recrystallization at low temperature (−20 °C) from CH_2Cl_2/pentane (1:3) gave 0.195 g (80% yield) of **3**$^+$. Anal. Calcd for $C_{120}H_{120}F_6Fe_3P_7{\cdot}7/4CH_2Cl_2$: C, 66.19, H, 5.63. Found: C, 66.00, H, 5.87.

[{Cp*(dppe)Fe(CC−)}$_3$(1,3,5-C$_6$H$_3$)][PF$_6$]$_2$ (3^{2+}). As described above 0.255 g (0.13 mmol) of **3** in 30 mL of CH_2Cl_2 was reacted with 0.086 g (2.0 equiv) of ferricinium hexafluorophosphate. The dark green powder of **3**$^{2+}$ was dried under vacuum. Recrystallization at low temperature (−20 °C) from CH_2Cl_2/pentane (1:3) gave 0.230 g (80% yield) of **3**$^{2+}$. Anal. Calcd for $C_{120}H_{120}F_{12}Fe_3P_8{\cdot}7/4CH_2Cl_2$: C, 65.35, H, 5.48. Found: C, 64.89, H, 5.69.

X-ray Crystallography for 2^+. Crystals suitable for single X-ray diffraction studies were obtained from CH_2Cl_2/pentane at −18 °C. The data were measured on a CAD-4 Enraf-Nonius automated diffractometer. All of the calculations were performed on a Digital MicroVax 3100 computer with the MOLEN package. Crystal data collection and refinement parameters are collected in Table 1. After Lorenz and polarization corrections,[61] the structure was solved with SIR-97,[62] which revealed the non-hydrogen atoms of the cation. During the refinements, two molecules of dichloromethane and the PF_6 anion appeared as statistically disordered on two positions in the ratio 80/20. The whole structure was refined with SHELXL97[63] by full-matrix least-squares techniques (use of F magnitude; x, y, z, β_{ij} for Fe, P, and C atoms of the cation, isotropic mode for the anion and solvent, x, y, z in riding mode for H atoms). The atom scattering factors were taken from the International Tables for X-ray Crystallography, and the ORTEP view was drawn with PLATON98.[64] All calculations were performed on a Pentium II computer.

Density Functional Calculations. Density functional calculations were carried out on different models using the Amsterdam Density Functional (ADF) program[65] developed by Baerends and co-workers.[66−69] The Vosko−Wilk−Nusair parametrization[70] was used for the local density approximation (LDA) with gradient corrections for exchange (Becke88)[71] and correlation (Perdew86).[72] The geometry optimization procedure was based on the method developed by Versluis and Ziegler.[73] The atom electronic configurations were described by a double-ζ Slater-type orbital (STO) basis set for H 1s, C 2s and 2p, P 3s and 3p, augmented with a 3d single-ζ function for the carbon atoms of the bis- or tris(ethynyl)benzene ligand. A triple-ζ STO basis set was used for Fe 3d and 4s, augmented with a single-ζ 4p function. A frozen-core approximation was used to treat the core electrons of C, P, and Fe. Geometries were partially optimized in order to reduce computational effort. C_s and C_{3v} symmetry was applied to calculations on "full-symmetry" models **2-H**$^+$ and **3-H**$^{+/2+}$, respectively. Calculations using the broken-symmetry formalism,[74−76] which consists of removing all the symmetry elements connecting the metal centers and imposing an asymmetry in the starting metal spin density, were carried out in C_1 symmetry for both **2-H**$^+$ and **3-H**$^{+/2+}$.

Acknowledgment. We are grateful to Prof. M. I. Bruce (Adelaide) and Dr. F. Paul (Rennes) for stimulating discussions and A. Mari (LCC, Toulouse) for Mössbauer measurements. L.C. and T.W. are indebted to ANRT and Laboratoires Standa (Caen) for financial support and a thesis grant to T.W. K.C. and J.-F.H. thank the Centre de Ressources Informatiques (CRI) of Rennes and the Institut de Développement et de Ressources en Informatique Scientifique (IDRIS-CNRS) of Orsay for computing facilities.

Supporting Information Available: X-ray crystallographic files, in CIF and PDF formats, for compound **2**$^+$ are available free of charge via the Internet at http://pubs.acs.org.

OM000341L

(61) Spek, A. L. *HELENA. Program for the handling of CAD4-diffractometer output SHELX(S/L)*; Spek, A. L., Ed.; Utrecht University: Utrecht, The Netherlands, 1997.
(62) Altomare, A.; Burla, M. C.; Camali, M.; Cascarano, G.; Giacovazzo, C.; Guagliardi, A.; Moliterni, A. G. G.; Polidori, G.; Spagna, R. *J. Appl. Crystallogr.* **1998**, *31*, 74.
(63) Sheldrick, G. M. *SHELX93. Program for Refinement of Crystal Structures*; Sheldrick, G. M., Ed.; University of Göttingen: Göttingen, Germany, 1993.
(64) Spek, A. L. *PLATON. A multipurpose crystallographic tool*; Spek, A. L., Ed.; Utrecht University: Utrecht, The Netherlands, 1998.
(65) *Amsterdam Density Functional (ADF) Program*, release 2.0.1; Vrije Universteit: Amsterdam, The Netherlands, 1996.
(66) Baerends, E. J.; Ellis, D. E.; Ros, P. *Chem. Phys.* **1973**, *2*, 41.
(67) Baerends, E. J.; Ros, P. *Int. J. Quantum Chem.* **1978**, *S12*, 169.
(68) Boerrigter, P. M.; Te Velde, G.; Baerends, E. J. *Int. J. Quantum Chem.* **1988**, *33*, 87.
(69) Te Velde, G.; Baerends, E. J. *J. Comput. Phys.* **1992**, *99*, 84.
(70) Vosko, S. D.; Wilk, L.; Nusair, M. *Can. J. Chem.* **1990**, *58*, 1200.
(71) Becke, A. D. *Phys. Rev.* **1988**, *A38*, 3098.
(72) Perdew, J. P. *Phys. Rev.* **1986**, *B34*, 7406.
(73) Verluis, L.; Ziegler, T. *J. Chem. Phys.* **1988**, *88*, 322.
(74) Noodleman, L.; Norman, J. G. J. *J. Chem. Phys.* **1979**, *70*, 4903.
(75) Noodleman, L. *J. Chem. Phys.* **1981**, *74*, 5737.
(76) Noodleman, L.; Case, D. A. *Adv. Inorg. Chem.* **1992**, *38*, 423.